ARTICLE IN PRESS

Advanced Engineering Informatics xxx (2015) xxx–xxx

Contents lists available at ScienceDirect

Advanced Engineering Informatics

journal homepage: www.elsevier.com/locate/aei

Improved digital photogrammetry technique for crack monitoring

Satoshi Nishiyama [a,*], Nao Minakata [b], Teruyuki Kikuchi [c], Takao Yano [b]

[a] Graduate School of Environmental and Life Science, Okayama University, Okayama 700-8530, Japan
[b] Graduate School of Engineering, Kyoto University, Kyoto 615-8540, Japan
[c] JP Design Co., Ltd., Tokyo 101-0021, Japan

ARTICLE INFO

Article history:
Received 21 May 2014
Received in revised form 13 May 2015
Accepted 22 May 2015
Available online xxxx

Keywords:
Photogrammetry
Image processing
Perspective projection
Crack displacement
Tunnel

ABSTRACT

Inspections to evaluate the safety, durability, and service life of aging infrastructure play an important role in determining the countermeasures that need to be taken, such as reinforcement, repair, and reconstruction. In infrastructure containing concrete, such as bridges and tunnels, crack widths and patterns on surfaces are two of the most important signs used to estimate durability. Current conventional techniques used for this purpose suffer from challenges such as tediousness, subjectivity, and high cost. Consequently, a new measurement technique that overcomes these challenges while measuring crack displacement with high accuracy and precision in aging civil engineering structures is needed. In this paper, we proposed a technique for measuring crack displacement using a digital camera image. In the proposed technique, reflective targets are established around both sides of a crack as gauges, and subsequent digital camera images of the targets are subjected to image processing to determine the displacements of the targets. These displacements can be measured using images captured from any arbitrary camera position. The results of experiments conducted to verify the efficacy of the proposed method show that crack displacements of less than 0.10 mm can be measured with high accuracy and precision using digital images captured at a distance of 10.0 m from the target, while less than 0.20 mm changes in the tensile displacement of the crack can be measured from an image captured at 25.0 m from the crack. Measurement results obtained from a tunnel are also presented to show that cracks in the walls of an actual tunnel can be identified through simple measurements. These measurements, taken over a period of one year, indicate that the tendency of crack displacement and slide movements are in close agreement.

1. Introduction

Much of the infrastructure in Japan was developed during the period of rapid economic growth in the 1960s. Some of the structures involved are now more than 50 years old; consequently, it is essential that they be monitored in order to ensure that they are safe [1,2]. Inspections to evaluate the durability and service life of such infrastructure play an important role in determining the countermeasures that need to be taken, such as reinforcement, repair, and reconstruction. In infrastructure containing concrete, such as bridges and tunnels, crack widths and patterns on surfaces are two of the most important signs used to estimate their durability. To measure the change in crack width and to prevent resultant damage, it is necessary to establish techniques for monitoring the crack behavior (e.g., [3,4]). Most existing approaches in this area are hand-sketch based, and crack openings are often evaluated using measuring magnifiers or crack width rulers; therefore, conventional measurement methods are manual, which may lead to nonobjective evaluation. Fiber optic sensors are also being used for crack monitoring. This technique does not utilize visual inspection and achieves measurements with accuracy similar to the standard strain gauges and extensometers; however, the cost of the data readout equipment used in applications coupled with installation and connection of the acquisition systems is very high (e.g., [5,6]). In contrast to wired systems, wireless systems require no cables for data transfer and are known for their low cost of deployment; however, their lifetime is limited by their battery-operated sensing devices (e.g., [7,8]).

This paper proposes a new crack monitoring measurement technique based on digital image processing and photogrammetry that overcomes the challenges outlined above. A variety of digital image processing technology based measurement systems have been developed. The majority of these systems recognize the number of the pixels in a crack image reflected in the image as the crack width, and utilize image processing techniques such as binarization processing to facilitate counting of the number of the pixels in the crack image [9–13]. However, because the pixels of the crack

* Corresponding author. Tel.: +81 86 251 8152; fax: +81 86 251 8866.
E-mail address: nishiyama.satoshi@okayama-u.ac.jp (S. Nishiyama).

http://dx.doi.org/10.1016/j.aei.2015.05.005
1474-0346/

Please cite this article in press as: S. Nishiyama et al., Improved digital photogrammetry technique for crack monitoring, Adv. Eng. Informat. (2015), http://dx.doi.org/10.1016/j.aei.2015.05.005

image reflected in the image vary significantly depending on the photographing conditions, especially lighting, it is difficult to measure the change in crack width with high accuracy in the actual field. Moreover, photogrammetry based measurement systems are not very popularity because it utilizes a complicated process in which images need to be taken from various camera positions [14–17].

In our proposed technique, reflective targets are established as gauges at measurement points along both sides of a crack, and the two-dimensional displacement of the crack—tensile and shear displacement—is calculated based on the coordinates of these targets using only one image, captured from any arbitrary position.

(1) Measurement can be performed using only a digital camera, reflective targets, and a PC, keeping costs very low, as low as that of the conventional photogrammetry method. However, unlike the conventional photogrammetry method, measurement is performed using only one captured image, as opposed to multiple images being required.
(2) The measurement values of the crack width can be calculated independent of the lighting conditions, unlike the conventional image processing method, because the proposed technique recognizes the distances between the circles of the targets as the crack width.

The results of experiments conducted verify the measurement accuracy of the proposed method in its determination of the relation between the distance and the angle of photographic positions from the targets. Further, we present the measurement results for crack displacements in a tunnel damaged by a landslide to demonstrate that the durability of an infrastructure can be identified through simple measurements.

2. Principle of crack measurement

This section explains the proposed technique and the principle for measuring cracks from digital images. This proposed technique can be used to measure the width of a crack without detecting the crack itself [18].

2.1. Measurement process

The width of a crack is measured as follows:

(1) Reflective targets are installed around the crack as gauges, as shown in Fig. 1 [19]. These targets are designed with four glass beads arranged in circles to induce the strong diffuse reflection of incident light. The size of the target changes according to the distance between the photographic position and the target. The four circles on one target is used for markers for perspective projection that is explained later, and one pair of circles on both sides of the crack is used for measuring the change in crack width. The distance between one pair of circles on both sides of the crack is measured, with the change in the distance indicating the displacement.
(2) A digital image of the targets is captured from an arbitrary camera position and angle. The captured digital image is then converted to one facing the target via perspective projection [20].
(3) The two-dimensional coordinate of the centroids of the circles in the image are measured via image processing.
(4) The distances between the circles of the targets on both sides of the crack indicate the tensile and shear displacements.

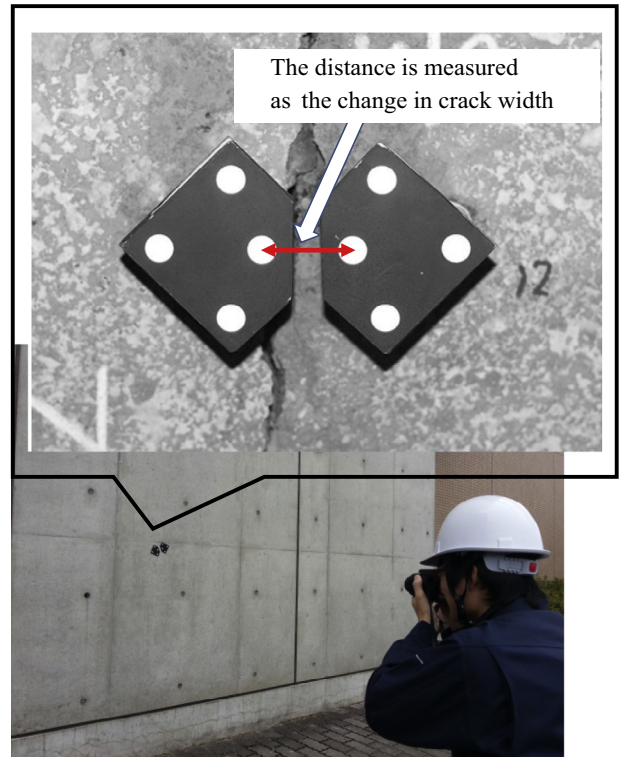

Fig. 1. Capturing a digital image of the targets from an arbitrary position. Reflective targets are established on both sides of a crack.

This measurement procedure has the following characteristics:

(1). It involves only photographs and eliminates the need for human expertise to improve accuracy, as required in conventional measurement techniques.
(2). It requires only a digital camera, targets, and a PC, which reduces cost.

2.2. Basic principles of target coordinate measurement

Image processing is used to simplify identification of the centroids of circles in the images. The measurement accuracy/precision of the system strongly depends on that of the two-dimensional coordinates of the centroids of the circles on the targets as measurement points [21]. Therefore, to improve this two-dimensional measurement accuracy/precision, reflective targets arranged in circles are established at the measurement points. The glass beads can induce the strong diffuse reflection of light. The digital imageries are categorized into gauge imageries in white and other areas in black through binarization using a certain threshold intensity that is less than half the maximum value. Fig. 2 illustrates the distribution of the intensity distribution of the circle. The multiple lines in the right figure represent various examples of the intensity distribution displayed in a two-dimensional section, and the red line is an example of the threshold intensity for binarization. The white areas are calculated based on a binary image acquired by the binarization processing, but the diameter of the circle should be fairly large, at least 20 pixels or bigger with a uniform pattern by adjusting the photographing condition.

The two-dimensional coordinates of the centroids are obtained by calculating the center of gravity of the white areas in each circle to obtain the centroid even in an elliptical shape. Assuming that the x- and y-coordinates are $x = 1–n$ and $y = 1–m$ in the image coordinate system, the coordinates (x, y) of the gauge imageries are

Please cite this article in press as: S. Nishiyama et al., Improved digital photogrammetry technique for crack monitoring, Adv. Eng. Informat. (2015), http://dx.doi.org/10.1016/j.aei.2015.05.005

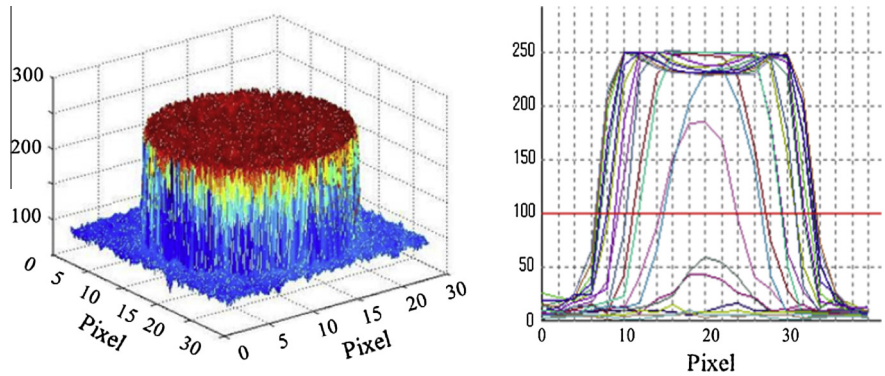

Fig. 2. Intensity value distribution of the circle on the target. The vertical axis represents the intensity value. The horizontal axis represents the pixel number of the circle on the target.

calculated using the following equation. In other words, the coordinates of the centroids of the circles in the images are obtained by calculating the center of gravity of a particular imagery's gauge.

$$x = x_0 + a_x \frac{\sum_{i=1}^{n}\sum_{j=1}^{m}(q(i,j)\times x_{ij})}{\sum_{i=1}^{n}\sum_{j=1}^{m} q(i,j)}$$
$$y = y_0 + a_y \frac{\sum_{i=1}^{n}\sum_{j=1}^{m}(q(i,j)\times y_{ij})}{\sum_{i=1}^{n}\sum_{j=1}^{m} q(i,j)} \quad (1)$$

where x_0 and y_0 denote the origin of the image coordinate system, a_x and a_y denote the pixel size, and $q(i, j)$ is the intensity value of pixel(i, j).

Next, the image seen from the front view of the targets is calculated using the perspective projection [22,23]. Perspective projection is based on the collinearity condition, in which a measurement point, the camera, and the measurement point's imagery appearing in the captured image are connected by a straight line. The concept of collinearity condition is illustrated in Fig. 3. In the figure, there are two coordinate systems: the image coordinate xy system, which originates from the center of the image and is in line with the axis of the digital camera's CCD or CMOS array; and the camera coordinate system xyz system, consisting of x and y axes as well as the optic z axis, which originates from the center of the lens and is parallel to the image coordinate system. The object is on the XYZ ground coordinate system. The light from measurement point P on the object goes through the center of lens O and focuses into imagery p. Considering the geometric relation between these elements, the measurement point, lens, and imagery are aligned. The coordinates of the measurement point P, viewed from the camera coordinate system xyz, and the

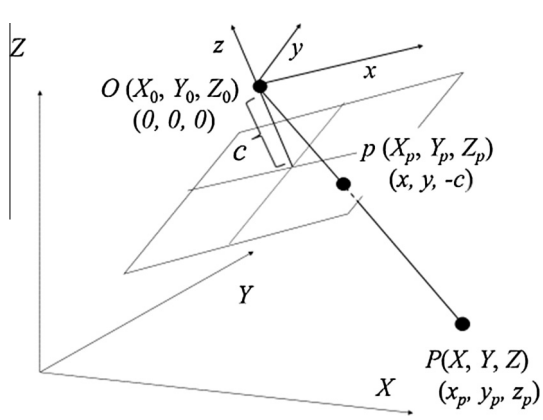

Fig. 3. Illustration of the collinearity condition.

coordinate values of the measurement point's imagery p viewed from the camera coordinate system are assumed to be $P(x_p, y_p, z_p)$ and $p(x, y, -c)$, respectively. Here, the focal length of the camera is denoted by c. Using matrix R, which represents the rotation of the coordinate axis, and the coordinates for $O(X_0, Y_0, Z_0)$ on the ground coordinate system originating from the center of the lens $O(0, 0, 0)$ on the camera coordinate, the relation between the ground coordinate system point $p(X_p, Y_p, Z_p)$ and the ground coordinate system point $P(X, Y, Z)$ is given as follows:

$$(X - X_0)/(X_p - X_0) = (Y - Y_0)/(Y_p - Y_0) = (Z - X_0)/(Z_p - X_0)$$
$$R(x, y, -c)^T = (X_p - X_0, Y_p - Y_0, Z_p - Z_0)^T \quad (2)$$

Assuming that when the y, x, and z axes are rotated sequentially in the right-hand screw direction by ω, φ and κ, respectively, around the camera coordinate system that has no inclination, they serve as the camera axes with a given inclination upon photographing, the rotational angle of coordinate axis R is given as follows:

$$R = \begin{bmatrix} 1 & 0 & 0 \\ 0 & \cos\omega & -\sin\omega \\ 0 & \sin\omega & \cos\omega \end{bmatrix} \begin{bmatrix} \cos\varphi & 0 & \sin\varphi \\ 0 & 1 & 0 \\ -\sin\varphi & 0 & \cos\varphi \end{bmatrix} \begin{bmatrix} \cos\kappa & -\sin\kappa & 0 \\ \sin\kappa & \cos\kappa & 0 \\ 0 & 0 & 1 \end{bmatrix} \quad (3)$$

Representing the elements of the rotation matrix by m_{ij}, Eq. (2) is transcribed to collinearity condition equations described by the following equation:

$$x = -c\frac{m_{11}(X - X_0) + m_{12}(Y - Y_0) + m_{13}(Z - Z_0)}{m_{31}(X - X_0) + m_{32}(Y - Y_0) + m_{33}(Z - Z_0)}$$
$$y = -c\frac{m_{21}(X - X_0) + m_{22}(Y - Y_0) + m_{23}(Z - Z_0)}{m_{31}(X - X_0) + m_{32}(Y - Y_0) + m_{33}(Z - Z_0)} \quad (4)$$

Because the coordinates of the reflective target are two dimensional values, the coordinates of Z become constant. Eq. (4) is nonlinear, and we rewrite the collinearity condition equations to the linear equation as follows:

$$x = \frac{b_1X + b_2Y + b_3}{b_7X + b_8Y + 1} \qquad y = \frac{b_4X + b_5Y + b_6}{b_7X + b_8Y + 1} \quad (5)$$

There are eight unknowns in total; specifically, b_i (i = 1–8) representing the camera position and angle. Eq. (5) shows the relation between the coordinates (X, Y) in the original image coordinate system and the coordinates (x, y) in the image coordinate system seen from the front view of the targets as shown in Fig. 4. Since Eq. (5) is established for one known point, four or more known points are required to solve these equations. A reflective target

Please cite this article in press as: S. Nishiyama et al., Improved digital photogrammetry technique for crack monitoring, Adv. Eng. Informat. (2015), http://dx.doi.org/10.1016/j.aei.2015.05.005

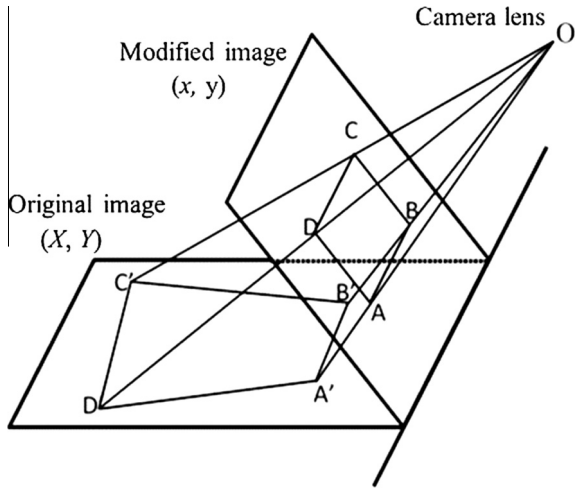

Fig. 4. Illustration of perspective projection.

installed around the crack is designed with four circles, as shown in Fig. 1. The *XY* coordinates of the four circles are printed on the precisely established positions, and the *XY* coordinates are quantities known in advance. Moreover, the corresponding *xy* coordinates of the four circles on the target can be automatically measured by calculating the center of gravity of the imagery's gauges. By using the known quantities, the unknown b_i in Eq. (5) is automatically obtained by the least-squares method. Then, the *xy* coordinates of the centers of the four circles shown in Fig. 5 are automatically substituted for (*X*, *Y*) in Eq. (5). By a series of procedures, a digital image captured at an arbitrary camera angle is automatically converted to one facing the target via perspective projection. Finally, the distance between the pair of circles on both sides of the crack is also automatically calculated, and the change in the distance is evaluated as the crack width [24,25]. Thus, the proposed method does not measure the crack itself but the target installed around the crack. Setting up the target is a bit complicated, but this method has the following advantages:

(1) It is capable of measuring the crack width under various conditions without being dependent on any one condition, such as lighting. Further, it measures the changes in crack width with high accuracy both close to and at a distance from the crack. Conventional measurement methods, such as the conventional image processing method, do not have this advantage as they have to conduct binarization processing after imaging the crack.
(2) It is able to accurately measure the change in crack width by simply taking one image from any photographing position. Thus, measurement can be performed in real time through complete automation after taking an image. This is in direct contrast to conventional methods that utilize the principle of close range photogrammetry, which requires multiple images taken from various photographing positions.

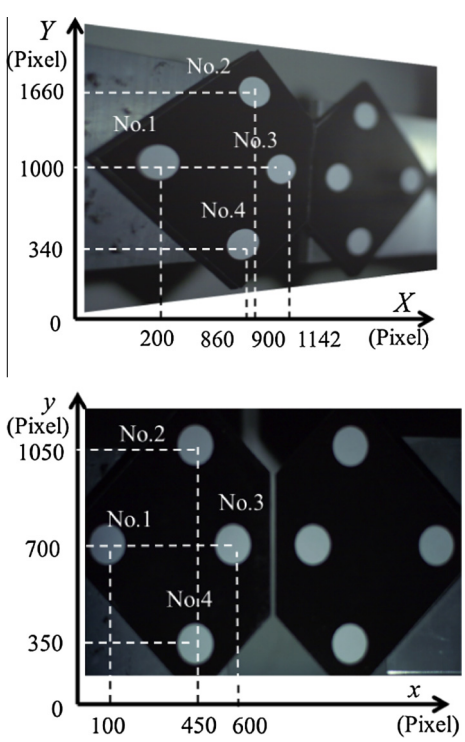

Fig. 5. *XY* coordinates at the centers of the four circles. These coordinates are substituted for (*x*, *y*).

3. Experiments and discussion

We conducted a number of experiments to evaluate the accuracy and precision of the proposed measurement system. The measurement errors of the coordinates of the centroids affect the accuracy and precision of this system. The size of the imagery of the target appearing on the captured image decreases with increase in the distance between the photographic position and the target. The measurement errors of the coordinates of the centroids depend on the size of the imagery of the target. Further, increasing the camera angle also causes an increase in the measurement errors of the coordinates of the centroids. Therefore, we measured the relation between the accuracy and the precision of the displacement measurement, camera positions, and camera angle. All images were captured using a 13 MP digital camera.

To verify the measurement accuracy and precision, a reflective target was placed at a fixed position, another glued to a micrometer, and digital images captured at various camera positions and camera angles shown in Fig. 6.

The distance of the micrometer's artificial movement D_0 and measured displacement *D* using the captured images were then obtained to calculate the differences between the two. Accuracy is defined as the average of the difference between D_0 and the measured displacement *D*, and precision is defined as the measurement value's dispersion. Eq. (6) gives the measurement accuracy and precision, respectively. It is possible to improve the accuracy and precision by using the plural-time measurement data, which give

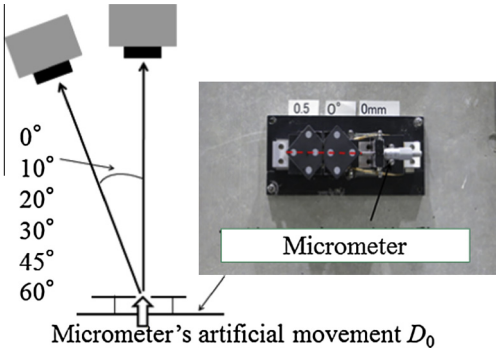

Fig. 6. Camera positions and camera angles used in the experiments. (Fixed target and target displaced by a micrometer.)

Please cite this article in press as: S. Nishiyama et al., Improved digital photogrammetry technique for crack monitoring, Adv. Eng. Informat. (2015), http://dx.doi.org/10.1016/j.aei.2015.05.005

the value of n as two or more in Eq. (6). Fig. 6 shows the camera positions L and camera angles α used in the experiments.

$$\text{Accuracy} = \sqrt{\frac{(D - D_0)^2}{n}} \quad \text{Precision} = \sqrt{\frac{\sum\left(D - \frac{\sum_{i=1}^{n} D}{n}\right)^2}{n}} \tag{6}$$

Fig. 7 and Table 1 show the relation between the distance of the micrometer's artificial movement D_0 and the measured displacement D. All images were captured at a camera angle of 0° and focal length 50.0 mm. Increasing L caused deterioration of the accuracy and precision of the measurement value; however, the displacement could be measured with accuracy/precision of less than 0.02 mm when capturing images at up to 1.0 m distance from the targets.

Fig. 8 and Table 2 show the relation between the camera angle, α, and the accuracy and precision. When the distance between the camera position and the target is long, the measurement results are not affected by the camera angle. Therefore, the images were captured at a camera position of 0.36 m. At different camera angles, α, when the images are captured at a camera angle less than 20°, the displacements could be measured with good accuracy/precision of 0.10 mm. Increasing the camera angle, α, caused deterioration of the accuracy and precision of the measured value. When camera angle α was 60°, the accuracy deteriorated by 0.05 mm and the precision by 0.01 mm. In the above experiments, all images were captured under short-distance photographing conditions. In real life, images may have to be captured at distances of more than 1.5 m from the targets. From Table 1, it can be estimated that the accuracy/precision is proportional to the distance between the camera and the target, L. When the distance between the camera and the target, L, exceeds 1.5 m, the measurement accuracy/precision decreases because the diameter of the circles in the images become small. For a long-distance photographing condition, it is necessary to use larger targets. Therefore, to verify the effect of using a large target, two larger targets, two and eight times the size of the conventional target, were used in further experiments with a micrometer shown in Fig. 6. All images were captured at a camera angle of 0°, and a lens with focal length 300 mm was used.

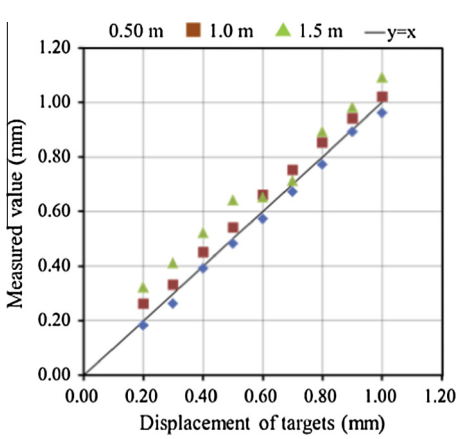

Fig. 7. Relation between the distance of the micrometer's artificial movement Do and the measured displacement D. Points are the relation between the displacement of targets and the measured value. The values of distance in the figure signify the distance between the camera and the target.

Table 1
Relation between accuracy/precision and L. The target size is 50.0 × 50.0 mm and the focal length is 50.0 mm.

L	0.5 m	1.0 m	1.5 m
Accuracy (mm)	0.02	0.04	0.08
Precision (mm)	0.01	0.02	0.04

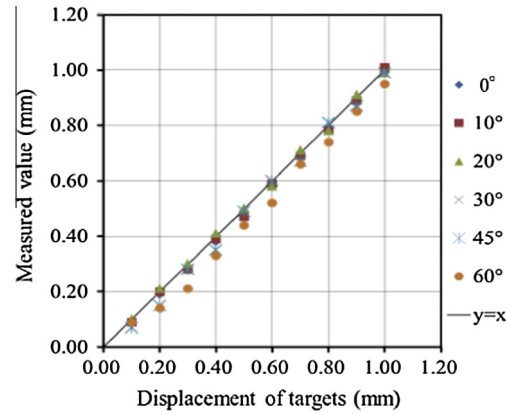

Fig. 8. Relation between camera angle and accuracy. The points are the relation between the camera angle and the measured value. The values of angle in the figure signify camera angle.

Table 2
Relation between accuracy/precision and α.

Camera angle α	0	10	20	30	45	60
Accuracy (mm)	0.01	0.01	0.01	0.03	0.02	0.06
Precision (mm)	0.01	0.01	0.01	0.01	0.02	0.02

Fig. 9 shows the relation between the accuracy and L (5.0–100.0 m) for targets with sizes two times (100.0 × 100.0 mm) and eight times (400.0 × 400.0 mm) larger than the original with a lens of 300 mm focal length. Table 3 shows the relation between the accuracy/precision and L (5.0, 7.0, 10.0, 15.0, and 20.0 m) for the target two times larger than the original with a lens of 300 mm focal length and shows the same for L exceeding 25.0 m and the target eight times larger than the original. It shows that the accuracy is 0.20 mm or less, although these results show that the accuracy/precision deteriorates with increase in L, which agrees with the results of the experiment detailed above. Tables 1 and 3 are summarized in Fig. 10. In the corresponding three experiments, both the distance between the camera and the target, L, and the target size and focal length were varied. Hence, the diameter of the circles in the images was used as the x-axis in

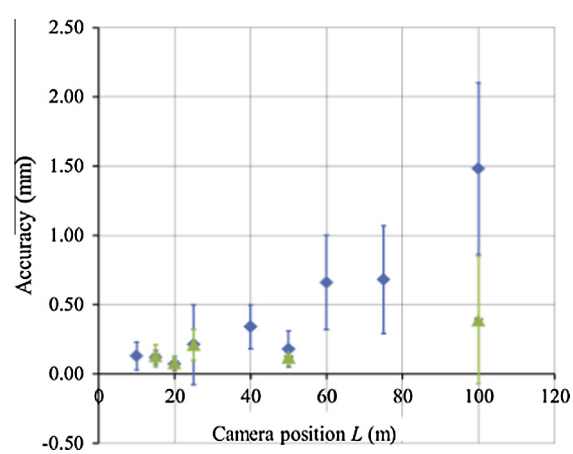

Fig. 9. Relation between accuracy/precision and L for targets with sizes two and eight times larger than the original. Diamonds and triangles indicate the 100.0 × 100.0 mm target and 400.0 × 400.0 mm target, respectively. Error bars in the figure mean the precision.

Please cite this article in press as: S. Nishiyama et al., Improved digital photogrammetry technique for crack monitoring, Adv. Eng. Informat. (2015), http://dx.doi.org/10.1016/j.aei.2015.05.005

Table 3
Relation between accuracy/precision and *L*. When *L* is less than 20.0 m, target size is 100.0 × 100.0 mm and focal length is 300.0 mm. When *L* is more than 25.0 m, target size is 400.0 × 400.0 mm and focal length is 300.0 mm.

L	5.0 m	7.0 m	10.0 m	15.0 m
Accuracy (mm)	0.07	0.11	0.07	0.20
Precision (mm)	0.06	0.09	0.04	0.14
L	20.0 m	25.0 m	50.0 m	100.0 m
Accuracy (mm)	0.15	0.11	0.33	0.57
Precision (mm)	0.11	0.07	0.25	0.46

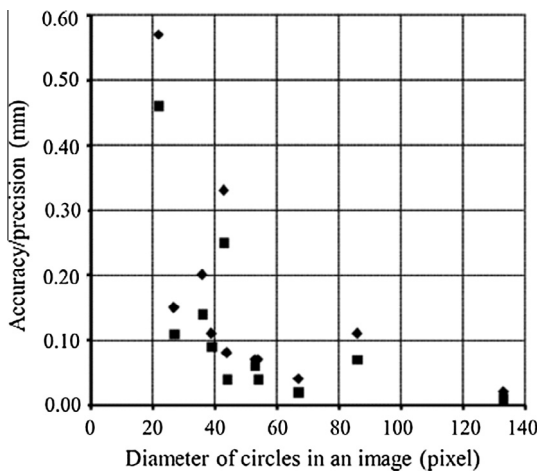

Fig. 10. Points indicate the relation between the diameter of the circles in the images and the measurement accuracy/precision. Diamonds and squares indicate accuracy and precision, respectively.

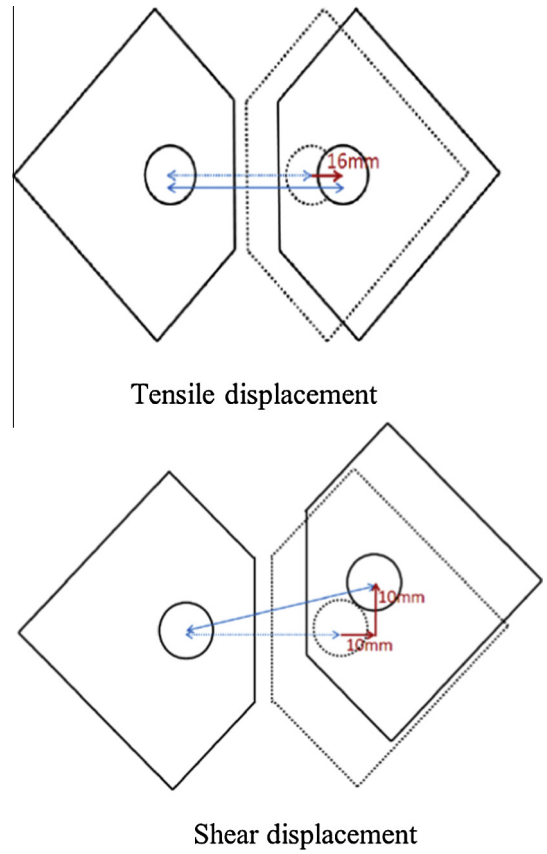

Fig. 11. Measurement of tensile and shear displacement. The upper figure shows the occurrence of only tensile displacement while the lower figure shows the simultaneous occurrence of both shear and tensile displacement. From the displacement measurements, it is determined whether only tensile displacement occurs.

Fig. 10. It is found that the smaller the diameter of the circles in the images, the less the accuracy/precision become, because the measurement accuracy/precision is concerned with the dispersion of analytical results of the center of gravity of the white areas in each circle by using Eq. (1). It is proved possible to take measurements with a high degree of accuracy and precision by using the targets in appropriate size corresponding to the photographing condition.

In general, visual inspection using a vernier caliper can be used to measure only the tensile displacement from the change in crack width. For a 16.0 mm displacement, we cannot determine whether only tensile displacement occurs when using conventional methods. Our proposed measurement system, in contrast, can measure both tensile and shear displacement, as shown in Fig. 11. Consequently, we performed another experiment to verify the accuracy and precision of the measured tensile and shear displacements. In the experiment, the targets with a size of 50.0 × 50.0 mm were attached to a micrometers shown in Fig. 6 and the accuracy/precision was obtained by measuring the distances for which the targets with micrometers moved. Table 4 gives a comparison of the accuracy and precision of the measured shear and tensile displacements. All images were captured at a camera angle of 0° and photogrammetric position of 0.5 m. The figures show that we can measure the shear and tensile displacements simultaneously with high accuracy and precision.

Table 4
Accuracy/precision of measured displacement *x* denotes tensile displacement and *y*, shear displacement.

	x	*y*
Accuracy (mm)	0.03	0.02
Precision (mm)	0.04	0.02

4. Measurement results for crack width in a tunnel

We applied the proposed method to crack measurement in tunnel constructed 20 years ago to prevent the occurrence of landslides by draining groundwater in a slope [26]. Extensometer measurements indicate a movement of 2.0–3.0 mm per year in the slope. Cracks in the tunnel therefore need to monitor for safety purposes [27,28]. Fig. 12 is a photograph of the tunnel, which was excavated at a depth of about 50.0 m below the surface, and has a diameter of about 2.0 m. The tunnel contains more than 300 cracks caused by landslides.

Fig. 13 is a diagram of the tunnel viewed directly from above. The positions of 30 representative cracks are shown in the figure. Boring records reveal the existence of a slide plane indicated by the black solid line in the figure. The slide plane intersects the tunnel at two points from the entrance. Spring water was observed coming from the cracks in the positions indicated by the numbers written in blue letters. Further, because a large quantity of lime has adhered to the tunnel wall, visual inspection is impossible. To investigate the durability of the tunnel quantitatively, we applied our crack measurement system and investigated the relation between the effect of slides and crack displacement. Targets were placed at 30 locations, and crack behaviors were measured every two months.

We present the crack measurement results for three targets in this paper Target No. 1 is located on a vertical crack at a point

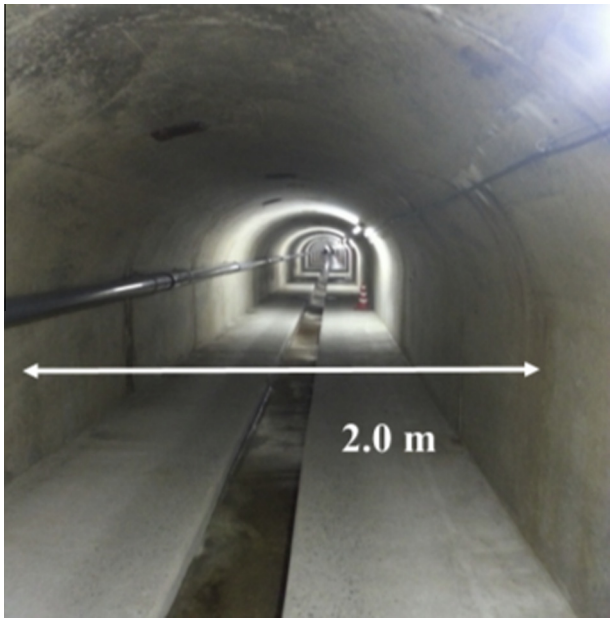

Fig. 12. Picture of the tunnel used in the experiment. We captured digital images of the targets at less than 0.5 m distance from the targets while hammering inspection.

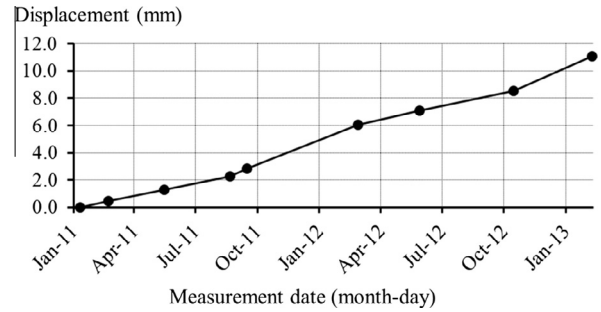

Fig. 14. Plot of changes in Target No. 1 crack width. +11.0 mm signifies that the crack is displaced by 11.0 mm in the tensile direction (tensile is positive).

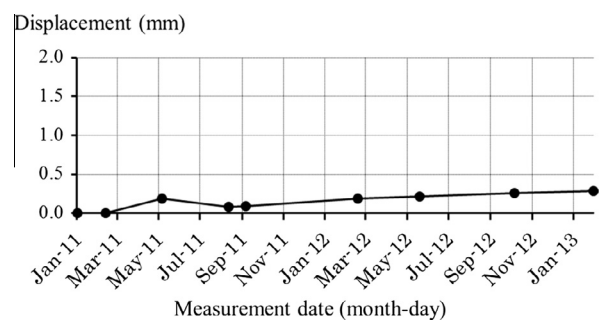

Fig. 15. Plot of changes in Target No. 4 crack width.

15.0 m from the entrance. Target No. 8 is also located on a vertical crack but in a branch tunnel at a point 300.0 m from the entrance. This target is directly under the slide plane, and therefore, there are more than 100 cracks around it. Target No. 4 is located on a horizontal crack near the slide plane at a point 100.0 m from the entrance. Figs. 14–16 show the results of changes in crack width measured using our system. Targets No. 1 and No. 8 are displaced at a constant pace over a period of one year. In contrast, Target No. 4 shows little displacement over that time period. It can therefore be concluded that cracks under the slide plane displace whereas others do not. This suggests that it is not necessary to monitor all of the more than 300 cracks, only the 10–20 cracks under the slide plane. The tensile displacement of Targets No. 1 and No. 8 is about 5.0 and 1.5 mm/year, respectively. The trend in the measured value of Target No. 1 agrees with that of extensometer measurements. The displacement of the target was found to correlate with the displacement caused by a shallow landslide.

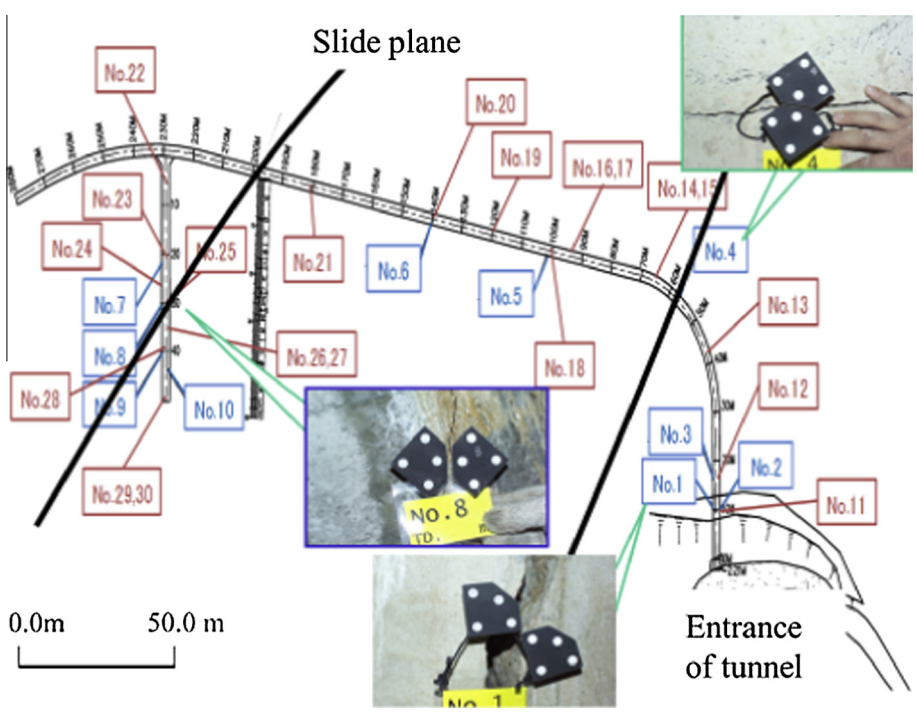

Fig. 13. Diagram of the tunnel viewed directly from above. Slide planes intersect the tunnel at Targets No. 1 and No. 8.

Please cite this article in press as: S. Nishiyama et al., Improved digital photogrammetry technique for crack monitoring, Adv. Eng. Informat. (2015), http://dx.doi.org/10.1016/j.aei.2015.05.005

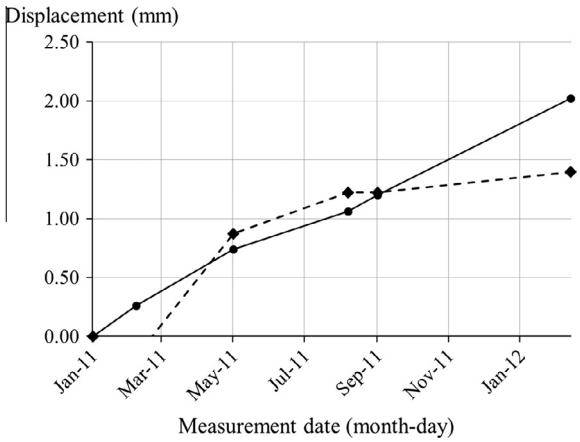

Fig. 16. Results of changes in crack width measured using our system. Diamonds and circles indicate the value measured using inclinometer and displacement of Target No. 8, respectively.

5. Conclusions

In this paper, we proposed a technique for measuring crack displacement using a digital camera image. In the proposed technique, reflective targets are established at measurement points around the crack as gauges and digital camera images of the targets are processed by photogrammetry and image processing. The results of experiments conducted to verify measurement accuracy and precision show that it is possible to take measurements with a high degree of accuracy/precision by adjusting the photographing condition of the proposed method, although a longer camera distance tended to produce slightly larger accuracies and precisions. In addition, measurement results obtained from an actual tunnel demonstrate that cracks in the tunnel wall can be identified through simple measurements. The measurements for a period of one year reveal that the tendency of crack displacement agrees with the extensometer measurement results. Furthermore, this result shows that measurement of only the cracks in the slide plane is adequate and the proposed method could reduce the labor and time required for conducting measurements.

There are still some things we have to settle to establish a new measurement system featuring simple measurement work and a high degree of accuracy/precision. In this paper, the targets were designed with microscopic glass beads arranged in four circles. Is it possible to obtain better accuracy/precision under similar photographing conditions by increasing the number of circles on the target? All images were captured using a 13 MP digital camera, but does our proposed measurement system allow free selection of the digital camera? When we compress digital image data at a high compression rate, does the measurement accuracy/precision change? We plan to do further research in response to the requirements of actual sites with the aim to complete the proposed measurement system.

References

[1] R. Morimoto, Estimating the benefits of effectively and proactively maintaining infrastructure with the innovative smart infrastructure sensor system, Socio-Econ. Plann. Sci. 44 (2010) 247–257.
[2] T. Asakura, Y. Kojima, Tunnel maintenance in Japan, Tunn. Undergr. Space Technol. 18 (2003) 161–169.
[3] I. Khan, R. François, A. Castel, Prediction of reinforcement corrosion using corrosion induced cracks width in corroded reinforced concrete beams, Cem. Concr. Res. 56 (2014) 84–96.
[4] G. Tiberti, F. Minelli, G.A. Plizzari, F.J. Vecchio, Influence of concrete strength on crack development in SFRC members, Cem. Concr. Compos. 45 (2014) 176–185.
[5] S. Villalba, J.R. Casas, Application of optical fiber distributed sensing to health monitoring of concrete structures, Mech. Syst. Signal Process. 39 (2013) 441–451.
[6] S. Yehia, T. Landolsi, M. Hassan, M. Hallal, Monitoring of strain induced by heat of hydration, cyclic and dynamic loads in concrete structures using fiber-optics sensors, Measurement 52 (2014) 33–46.
[7] K. Smarsly, K.H. Law, Decentralized fault detection and isolation in wireless structural health monitoring systems using analytical redundancy, Adv. Eng. Softw. 73 (2014) 1–10.
[8] S. Casciati, Z. Chen, A multi-channel wireless connection system for structural health monitoring applications, Struct. Contr. Health. Monit. 18 (5) (2011) 588–600.
[9] P.M. Dare, H.B. Hanley, C.S. Fraser, B. Riedel, W. Niemeier, An operational application of automatic feature extraction: the measurement of cracks in concrete structures, Photogramm. Rec. 17 (99) (2002) 453–464.
[10] U. Hampel, H.-G. Maas, Cascaded image analysis for dynamic crack detection in material testing, ISPRS J. Photogramm. Rem. Sens. 64 (2009) 345–350.
[11] T. Yamaguchi, S. Nakamura, R. Saegusa, S. Hashimoto, Image-based crack detection for real concrete surfaces, IEE J. Trans. Electr. Electron. Eng. 3 (2008) 128–135.
[12] G. De Schutter, Advanced monitoring of cracked structures using video microscope and automated image analysis, NDT&E Int. 35 (2002) 209–212.
[13] J. Valença, D. Dias-da-Costa, E. Júlio, Characterisation of concrete cracking during laboratorial tests using image processing, Constr. Build. Mater. 28 (2012) 607–615.
[14] S. Miura, S. Hattori, K. Akimoto, S. Nishiyama, Deformation monitoring of a slope by vision metrology, Int. Arch. Photogramm. Rem. Sens. Spatial Inform. Sci. 35 (Part B5) (2004) 64–69.
[15] R. Jiang, D.V. Jáuregui, K.R. White, Close-range photogrammetry applications in bridge measurement: literature review, Measurement 41 (2008) 823–834.
[16] Y. Ohnishi, S. Nishiyama, T. Yano, H. Matsuyama, K. Amano, A study of the application of digital photogrammetry to slope monitoring systems, Int. J. Rock Mech. Min. Sci. 43 (2006) 756–766.
[17] C.S. Fraser, B. Riedel, Monitoring the thermal deformation of steel beams via vision metrology, ISPRS J. Photogramm. Rem. Sens. 55 (2000) 268–276.
[18] N. Minakata, S. Nishiyama, T. Yano, T. Kikuchi, Study on crack monitoring method using digital photogrammetry, in: N. Yabuki, K. Makanae (Eds.), Proceedings of the First International Conference on Civil and Building Engineering Informatics, 2013, pp. 109–114.
[19] C.S. Fraser, S. Cronk, A hybrid measurement approach for close-range photogrammetry, ISPRS J. Photogramm. Rem. Sens. 64 (2009) 328–333.
[20] C. Laofor, V. Peansupap, Defect detection and quantification system to support subjective visual quality inspection via a digital image processing: a tiling work case study, Autom. Constr. 24 (2012) 160–174.
[21] C. Bernstone, A. Heyden, Image analysis for monitoring of crack growth in hydropower concrete structures, Measurement 42 (2009) 878–893.
[22] R. Jiang, D.V. Jáuregui, K.R. White, Close-range photogrammetry applications in bridge measurement: literature review, Measurement 41 (2008) 823–834.
[23] H.G. Sohn, Y.M. Lim, K.H. Yun, G.H. Kim, Monitoring crack changes in concrete structures, Comput.-Aid. Civ. Infrastr. Eng. 20 (2005) 52–61.
[24] L. Barazzetti, M. Scaioni, Crack measurement: development, testing and applications of an automatic image-based algorithm, ISPRS J. Photogramm. Rem. Sens. 64 (2009) 285–296.
[25] J. Valença, D. Dias-da-Costa, E. Júlio, H. Araújo, H. Costa, Automatic crack monitoring using photogrammetry and image processing, Measurement 46 (2013) 433–441.
[26] T.T. Wang, Characterizing crack patterns on tunnel linings associated with shear deformation induced by instability of neighboring slopes, Eng. Geol. 115 (2010) 80–95.
[27] C.H. Lee, Y.C. Chiu, T.T. Wang, T.H. Huang, Application and validation of simple image-mosaic technology for interpreting cracks on tunnel lining, Tunn. Undergr. Space Technol. 34 (2013) 61–72.
[28] S.N. Yu, J.H. Jang, C.S. Han, Auto inspection system using a mobile robot for detecting concrete cracks in a tunnel, Autom. Constr. 16 (2007) 255–261.